AGU PUBLICATIONS

JGR

Journal of Geophysical Research: Oceans

RESEARCH ARTICLE

10.1002/2017JC012921

Key Points:
- Water mass property changes along the DWBC reflect changes in deep convection in the Labrador Sea
- We find a first-order role for both advection along the DWBC and stirring with the interior
- Implied stirring is stronger south of the Flemish Cap

Correspondence to:
I. A. Le Bras,
ilebras@whoi.edu

Citation:
Le Bras, I. A., I. Yashayaev, and J. M. Toole (2017), Tracking Labrador Sea Water property signals along the Deep Western Boundary Current, *J. Geophys. Res. Oceans*, *122*, 5348–5366, doi:10.1002/2017JC012921.

Received 24 MAR 2017
Accepted 6 JUN 2017
Accepted article online 8 JUN 2017
Published online 3 JUL 2017

Tracking Labrador Sea Water property signals along the Deep Western Boundary Current

Isabela Astiz Le Bras[1,2], Igor Yashayaev[3], and John M. Toole[1]

[1]Department of Physical Oceanography, Woods Hole Oceanographic Institution, Woods Hole, Massachusetts, USA, [2]MIT-WHOI Joint Program in Physical Oceanography, Woods Hole, Massachusetts, USA, [3]Bedford Institute of Oceanography, Fisheries and Oceans Canada, Dartmouth, Nova Scotia, Canada

Abstract Observations of the Deep Western Boundary Current (DWBC) at Line W on the western North Atlantic continental slope southeast of Cape Cod from 1995 to 2014 reveal water mass changes that are consistent with changes in source water properties upstream in the Labrador Sea. This is most evident in the cold, dense, and deep class of Labrador Sea Water (dLSW) that was created and progressively replenished and deepened by recurring winter convection during the severe winters of 1987–1994. The arrival of this record cold, fresh, and low potential vorticity anomaly at Line W lags its formation in the Labrador Sea by 3–7 years. Complementary observations along the path of the DWBC provide further evidence that this anomaly is advected along the boundary and indicate that stirring between the boundary and the interior intensifies south of the Flemish Cap. Finally, the consistency of the data with realistic advective and mixing time scales is assessed using the Waugh and Hall (2005) model framework. The data are found to be best represented by a mean transit time of 5 years from the Labrador Sea to Line W, with a leading order role for both advection by the DWBC and mixing between the boundary flow and interior waters.

1. Introduction

The Deep Western Boundary Current (DWBC) carries cold, dense water from the high-latitude North Atlantic to the South Atlantic along the western boundary of the basin. The first indication of the DWBC appeared in water property measurements from the Meteor Expedition (1925–1927) in the Atlantic led by Alfred Merz and Georg Wüst [*Wüst*, 1935]. Many years later, the DWBC was confirmed by *Swallow and Worthington* [1961] near Cape Hatteras using acoustically tracked floats and hydrography.

Since those times, there have been many direct current measurements of this southward current using moored instrumentation: in the subpolar gyre at 53°N [*Dengler et al*., 2006; *Fischer et al*., 2010, 2015], at 47°N [*Rhein et al*., 2011; *Mertens et al*., 2014] and at the Grand Banks [*Schott et al*., 2004, 2006], close to the inter-gyre boundary at Line W at 39°N (Figure 1) [*Joyce et al*., 2005; *Toole et al*., 2011; *Peña-Molino et al*., 2012], at Cape Hatteras [*Pickart et al*., 1990], at 26.5°N [*Meinen et al*., 2013a; *Srokosz and Bryden*, 2015], at 16°N [*Kanzow et al*., 2006, 2008; *Köhler et al*., 2014] and in the Southern Hemisphere at 8°S and 11°S [*Dengler et al*., 2004; *Hummels et al*., 2015] as well as 34°S [*Meinen et al*., 2013b; *Dong et al*., 2014].

As North Atlantic deep waters spread equatorward in the DWBC, they subduct and are shielded from atmospheric forcing. Consequently, these waters can be tracked throughout the world ocean using their characteristic temperature and salinity properties, as well as anthropogenic tracer concentrations, such as chloroflourocarbons (CFCs), which are imprinted on them by the atmosphere at their source. Convectively formed water masses can also be tracked using potential vorticity (PV), a dynamical tracer that is conserved barring forcing and dissipation. Many studies have taken advantage of these unique tracer properties to track the spreading of North Atlantic deep water along the western boundary of the North Atlantic [e.g., *Lynn and Reid*, 1968; *Talley and McCartney*, 1982; *Molinari et al*., 1998; *Smethie et al*., 2000; *Stramma et al*., 2004; *LeBel et al*., 2008; *Kieke et al*., 2009; *Rhein et al*., 2015]. CFC studies of the DWBC, such as *Pickart et al*. [1989] have found along-boundary tracer spreading rates ($1-2\,\mathrm{cm\,s^{-1}}$) that are several times slower than mean speeds in the DWBC ($5-10\,\mathrm{cm\,s^{-1}}$), indicating stirring with the interior as well as recirculation. This discrepancy between effective spreading rates and mean DWBC speeds was also seen in analysis of acoustically tracked float data by *Bower and Hunt* [2000].

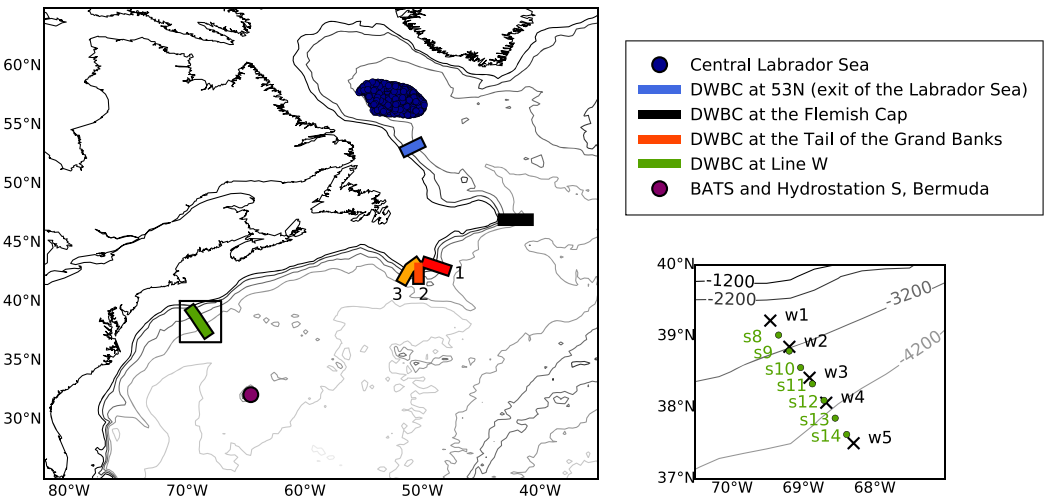

Figure 1. Map of data set locations along the path of the Deep Western Boundary Current as described in the legend. Three different cruise tracks (labeled 1–3) make up the data used at the Tail of the Grand Banks. Inset in the lower-right shows Line W mooring positions (in black) and station positions used in this study (in green). The Line W inset location is highlighted by a black square in the primary map. Isobaths starting at 200 m are contoured at 1000 m intervals, and labeled in the inset.

In this study, we interpret water mass property changes in the DWBC on the continental slope of New England (between 35°N and 40°N), where Line W moorings were operational from April 2001 to May 2014 (Figure 1). Line W is named for L. Valentine Worthington, for his many significant contributions to measuring and understanding North Atlantic current systems. Hydrographic surveys along Line W date back to 1994 and include measurements of anthropogenic tracers, such as CFCs and ^{129}I [*Smith et al.*, 2016]. In this work, we connect water mass property changes at Line W with upstream sources on interannual time scales. Previous work using this data set reported on DWBC transport measurements and variability on shorter time scales, including warm core rings shed from Gulf Stream meanders and deep cyclones [*Toole et al.*, 2011; *Peña-Molino et al.*, 2010; *Andres et al.*, 2015].

The DWBC is composed of water masses formed at high-latitude that are commonly identified by their source region and depth. The intermediate water masses in the DWBC are formed in the Labrador Sea (found at about 500–2000 m depth at Line W). Labrador Sea Water (LSW) is often split into lighter, upper LSW (uLSW) and denser, deep LSW (dLSW), which are formed under weaker and stronger forcing conditions, respectively [*Lazier*, 2001; *Stramma et al.*, 2004; *Kieke et al.*, 2006; *Rhein*, 2000; *Rhein et al.*, 2007]. In some years, dLSW may be formed in the center of the basin, while uLSW is formed in the boundary current [*Pickart et al.*, 1997]. The strength of the convection and corresponding water mass signature in the central Labrador Sea can vary dramatically from year to year, so that the distinction between upper and deep LSW is not always well defined or instructive [*Yashayaev*, 2007].

As an alternative to dividing LSW into upper and deep classes, LSW can be split into year-classes based on their history of formation and evolution. Four distinct LSW classes have been identified in the last three decades: $LSW_{1987–1994}$, $LSW_{2000–2003}$, LSW_{2008}, and $LSW_{2012–2016}$ [*Lazier et al.*, 2002; *Yashayaev*, 2007; *Yashayaev and Loder*, 2009, 2017, 2016]. In general, the density of a particular LSW class corresponds with the strength and persistence of winter cooling incurred through the years of its formation.

The $LSW_{1987–1994}$ water mass was formed during a period of extremely high North Atlantic Oscillation (NAO) index [*Lazier et al.*, 2002; *Hurrell*, 1995; *Marshall et al.*, 2001]. Intense cooling led to convection which reached 2500 m, forming a thick layer of homogeneous density, and consequently low PV. The resulting water mass was also anomalously fresh as low-salinity surface waters were mixed into the water column [*Yashayaev*, 2007]. Starting in the mid-1990s, winter cooling weakened, and the LSW classes formed over the subsequent years were generally shallower and less dense (Figure 2).

Our focus is on the density range of $LSW_{1987–1994}$, which we will label as dLSW here to highlight its extreme depth and density, as well as to connect with the literature [e.g., *Stramma et al.*, 2004]. The only record of this density range being ventilated in the Labrador Sea since 1960 was from 1987 to 1994 [*Yashayaev*,

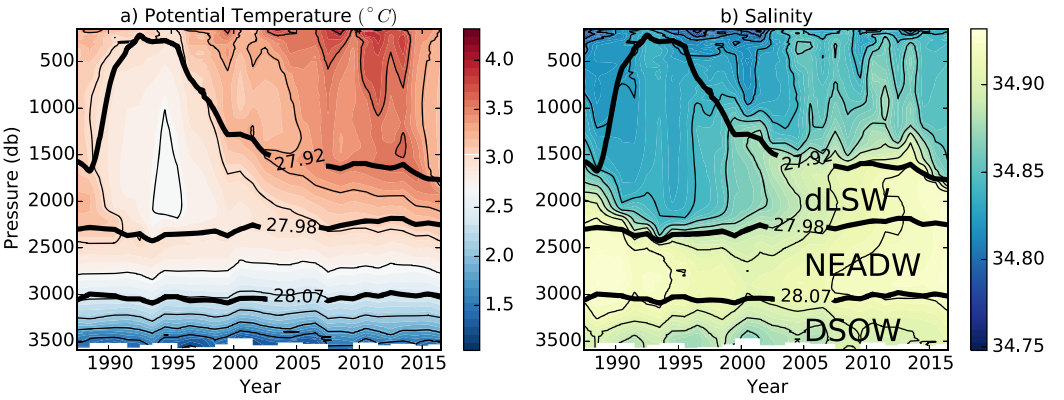

Figure 2. Time evolution of (a) potential temperature and (b) salinity profiles in the central Labrador Sea. Thick labeled lines highlight the neutral density boundaries between water masses. Water mass labels in Figure 2b apply to both panels (dLSW: deep Labrador Sea Water; NEADW: North East Atlantic Deep Water; DSOW: Denmark Strait Overflow Water). The dLSW layer is thickest, freshest, and coldest in the early/mid 1990s and becomes thinner, saltier, and warmer throughout the 2000s. At the end of the record, renewed strong convection is apparent as the water column cools and freshens to almost 2000 db.

2007]. This is the source of the strong water mass property variability that we track in this work. Our water mass density ranges are broadly consistent with others in the literature (Table 1). Although we generally describe bulk water mass properties, in section 4, we also analyze properties in small uniform bins of neutral density, independent of preset water mass definitions.

The densest water masses found in the DWBC are formed in the Nordic Seas. These waters flow over sills into the subpolar North Atlantic and are referred to collectively as Overflow Waters (OWs) [*Swift*, 1984; *Hansen and Osterhus*, 2000; *Dickson et al*., 2002]. OWs are separated into lighter Iceland-Scotland Overflow Waters (ISOW) and denser Denmark Strait Overflow Waters (DSOW), named for their origins. ISOW entrains saline Atlantic waters as it descends into the deep Icelandic basin and the resulting North East Atlantic Deep Waters (NEADW) contains only about 1/3 ISOW [*Van Aken and De Boer*, 1995; *Yashayaev et al*., 2007]. Because OWs enter the North Atlantic as narrow overflows and are significantly altered by entrainment, they do not have as significant a low PV signature in the subpolar gyre as LSW. Although OWs are not the focus of our analysis, we will refer to them (Table 1).

Building on the findings of DWBC tracer studies that indicated a role for stirring and recirculation in the spreading of deep water, recent work has investigated the relative importance of the DWBC versus interior pathways. In a sequence of float releases from 2003 to 2005, less than 10% of acoustically tracked isobaric floats seeded in the DWBC in the LSW layer at 50°N rounded the Tail of the Grand Banks in the DWBC, pointing to the importance of exchange between the boundary current and the interior as well as interior pathways [*Bower et al*., 2009, 2011, 2013]. Float deviations into the interior at the Grand Banks as well as the subsequent interior pathways were replicated in high-resolution models [*Gary et al*., 2011, 2012; *Lozier et al*., 2013]. However, seeding floats in the bottom-intensified core(s) of the DWBC is particularly challenging, adding uncertainty to the results of Lagrangian studies. There is mounting evidence from Eulerian

Table 1. Comparison of Water Mass Upper Boundary Definitions Used in kg m^{-3}: γ_n is Neutral Density and σ_2 is Potential Density Referenced to 2000 m[a]

	This Work	*Toole et al*. [2011] and *Peña-Molino et al*. [2010]	*Yashayaev et al*. [2007] and *Van Sebille et al*. [2011]
uLSW	γ_n=27.80 (160/690)		σ_2=36.5 (105/630)
dLSW	γ_n=27.92 (1180/1320)	γ_n=27.897(890/1100)	σ_2=36.82 (300/960)
NEADW	γ_n=27.98 (2300/1940)		σ_2=36.97 (2470/2150)
DSOW	γ_n=28.07 (3050/2790)		σ_2=36.98 (2550/2240)

[a]Each water mass extends to the upper boundary of the water mass directly below it in the table. uLSW, upper Labrador Sea Water; dLSW, deep Labrador Sea Water; NEADW, North East Atlantic Deep Water; DSOW, Denmark Strait Overflow Water. Values in parentheses are mean depths of the isopycnal in central Labrador Sea and at Line W in meter. When water mass boundaries are not listed, they are equivalent to those used in this work. Central Labrador Sea mean depths calculated from 1988 to 2013 and Line W mean depths calculated from w3 mooring data (November 2001 to May 2014).

observations that water mass signals can propagate in the DWBC effectively [*Stramma et al*., 2004; *Peña-Molino et al*., 2010; *Van Sebille et al*., 2011].

To assess the degree of connectivity in the DWBC, we compare salinity, potential temperature, and PV changes in the DWBC at Line W to changes in the Labrador Sea. In section 2, we introduce the Line W and central Labrador Sea data sets. This is followed, in section 3, by an analysis of Line W mooring data in θ-S space. We then turn to the shipboard data and quantify the correlation between Labrador Sea and Line W hydrographic anomalies in neutral density space (section 4). In section 5, we average within the dLSW density range and draw on additional observations of the DWBC (Figure 1) to further investigate the evolution of dLSW water mass properties along the DWBC. Finally, in section 6, we use the *Waugh and Hall* [2005] model to quantify the relative importance of advection and diffusion in dLSW spreading from the Labrador Sea to Line W. We discuss our results in section 7. Additional description of other water masses and the implementation of the *Waugh and Hall* [2005] model may be found in *Le Bras* [2017].

2. Data Sets

2.1. Line W

The Line W moored array consisted of five moorings (w1–w5) deployed on the continental slope southeast of Cape Cod from April 2004 to May 2014 spanning isobaths between 2200 and 4000 m, with the central mooring (w3) in the water since November 2001 (Figure 1). A sixth mooring was added to the array in May 2008, but does not enter our analysis as its water mass properties and variability are dominated by the Gulf Stream [*Peña-Molino et al*., 2010; *Andres et al*., 2015].

Between the two phases (2004–2008 and 2008–2014) of the Line W array, the distribution of moored instruments changed, complicating the construction of consistent time series. From 2004 to 2008, w1, w3, and w5 were equipped with McLane Moored Profilers (MMPs), profiling sensors which measure velocity, temperature, and conductivity, and moorings w2 and w4 were equipped with fixed instruments measuring velocity, temperature, and conductivity [*Toole et al*., 2011]. In the 2008–2014 setting, this distribution was reversed: w2 and w4 were equipped with MMPs and w1, w3, w5, and w6 were equipped with fixed instruments.

The MMPs typically sampled in bursts of 4 one-way profiles every 5 days. Averaging the individual profiles in these bursts in pressure space acts to filter out ageostrophic high-frequency signals because they were separated by 9.5 h, which is approximately half the local inertial and three-quarters of the semidiurnal tidal period [*Silverthorne and Toole*, 2009]; the resulting data set has 5 day temporal resolution and 2 db vertical resolution. The fixed instruments have much higher temporal resolution, 15 min for T/S and 15 or 30 min for velocity data, but their vertical resolution varies, and is on the order of 100 m.

To address the difference in temporal sampling, the fixed instrument data were low-pass filtered and subsampled to 5 day intervals, which is more than sufficient for the purposes of this study. Because of the irregular positions of fixed instruments (for the purposes of measuring DWBC transport), development of consistent vertical information across all of the moorings was more involved. For each mooring, the MMP data were subsampled at the mean positions of the fixed instruments that preceded or followed them. The subsampled data were then interpolated vertically using a cubic spline and the mean properties (temperature, salinity, PV, and velocity) within water mass boundaries described in Table 1 from the full and subsampled data sets were compared. Since the magnitude and variability of these water mass properties were well reproduced by the subsampled data, the subsampled MMP data set was used throughout to avoid measurement bias. The same cubic spline vertical interpolation was applied to the fixed sensor data.

Shipboard hydrographic measurements at fixed station positions which extend most of the way to Bermuda were occupied once or twice a year from 1994 to 1997 and 2001 to 2014 [*Andres et al*., 2015]. The hydrographic parameters used in this work represent a mean in neutral density space weighted by layer thickness of all stations that lie between the locations of moorings w1 and w5 (Figure 1) to facilitate comparison of moooring and hydrographic data.

2.2. Central Labrador Sea

An assemblage of ship stations and Argo float profiles are used to characterize the water properties around the epicenter of deep convection in the Labrador Sea based on winter hydrographic properties as described

in *Yashayaev and Loder* [2017, 2016] (Figure 1). This epicenter is bounded by the 3250 m isobath to the west and southwest. Each annual vertical profile was constructed by averaging temperature, salinity and pressure of all available vertically interpolated observations in σ_2 bins with $\Delta\sigma_2 = 0.005\,\mathrm{kg\,m^{-3}}$ over the central Labrador Sea domain. If any σ_2 bin did not have sufficient data points to form reliable estimates, its σ_2 limits were expanded incrementally until it included the needed number of observations or $\Delta\sigma_2$ reached $0.020\,\mathrm{kg\,m^{-3}}$. Further details of the calculations of robust seawater property statistics involving two types of statistical weights applied to the values in each σ_2 bin may be found in the "Methods and definitions A: Construction of time series" section of *Yashayaev* [2007]. The estimates found in the σ_2 bins were then vertically interpolated to 5 dbar, forming a uniform time-pressure array.

3. Water Mass θ-S Shifts at Line W Moorings

The Line W mooring θ-S properties lie between the central Labrador Sea θ-S properties and those observed at the Bermuda Atlantic Time Series (BATS) 75 km southeast of Bermuda (Figure 3). The waters formed by deep convection in the central Labrador Sea from 1987 to 1994 have a uniquely cold and fresh signature in the dLSW density range, so that large deviations in the cold-fresh direction can be assumed to emanate from the Labrador Sea. Their contribution to the θ-S properties can be seen in the cold-fresh curve visible in the shape of both the Line W and BATS data sets in the LSW density range (Figures 3 and 4) [*Curry et al*., 1998; *Phillips and Joyce*, 2007]. At BATS, θ-S properties are generally warmer and saltier than at Line W because of the influence of Mediterranean Water and the more circuitous path that LSW takes to get to BATS [*Talley and McCartney*, 1982; *Van Sebille et al*., 2011].

The dramatic changes in θ-S properties in the Labrador Sea from 1988 to 2014 are also illustrated in Figure 3. The extreme convection in the early 1990s resulted in a cold-fresh peak in the dLSW range. Thereafter, throughout the late 1990s and 2000s, the water in the dLSW range became warmer and saltier.

Peña-Molino et al. [2010, Figure 6] show that the annual mean θ-S properties at Line W's central mooring, w3, similarly change from cold-fresh to warm-salty within their dLSW layer from 2001 to 2008; reflecting the changes upstream in the Labrador Sea several years prior. This general pattern of warming and salinifying in the dLSW range continued at Line W to the end of the program, as evidenced by the data from moorings w1–w5. In addition to this continuing change in annual mean properties from cold-fresh to warm-salty, we show that there is a change in the range of θ-S properties present at Line W from year to year. In 2005, the θ-S properties measured over the year cover the full range of properties measured throughout the Line W record, from cold-fresh to warm-salty (Figure 4). This range progressively decreased and the annual mean became warmer and saltier in the LSW range. By 2013, the θ-S properties present were limited to the warm-salty edge of all sampled θ-S space. Because of our data subsampling and the fact that both MMP and fixed instrument measurements are present in both settings of the moored array, measurement bias has been minimized in this result.

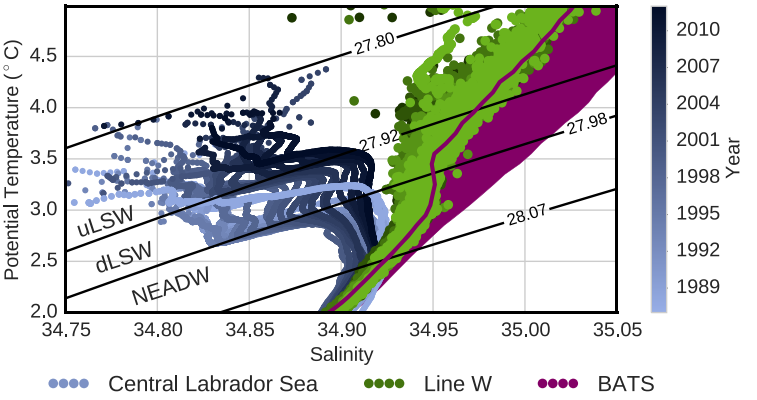

Figure 3. θ-S properties in the central Labrador Sea (blue), at Line W moorings (green), and BATS (magenta). Shades of green correspond to measurements at different Line W mooring sites as in Figure 4. Central Labrador Sea profiles are color-coded by year as specified in the colorbar. Line W mooring profiles include data from 2001 to 2014. BATS profiles include data from 1991 to 2015, measured monthly. Here we show the range of the 5th to 95th percentile of BATS measurements in salinity space, with the 5th percentile profile overlain, as it would otherwise be obscured by the Line W data points. Black lines are representative neutral density boundaries for 39°N and 1000 db.

This transition from a broad set of θ-S properties to a narrow distribution on the warm-salty edge of θ-S space is due to the decreasing presence of the water formed through intense deep convection in the central Labrador Sea in the early 1990s, which was anomalously fresh and cold. As

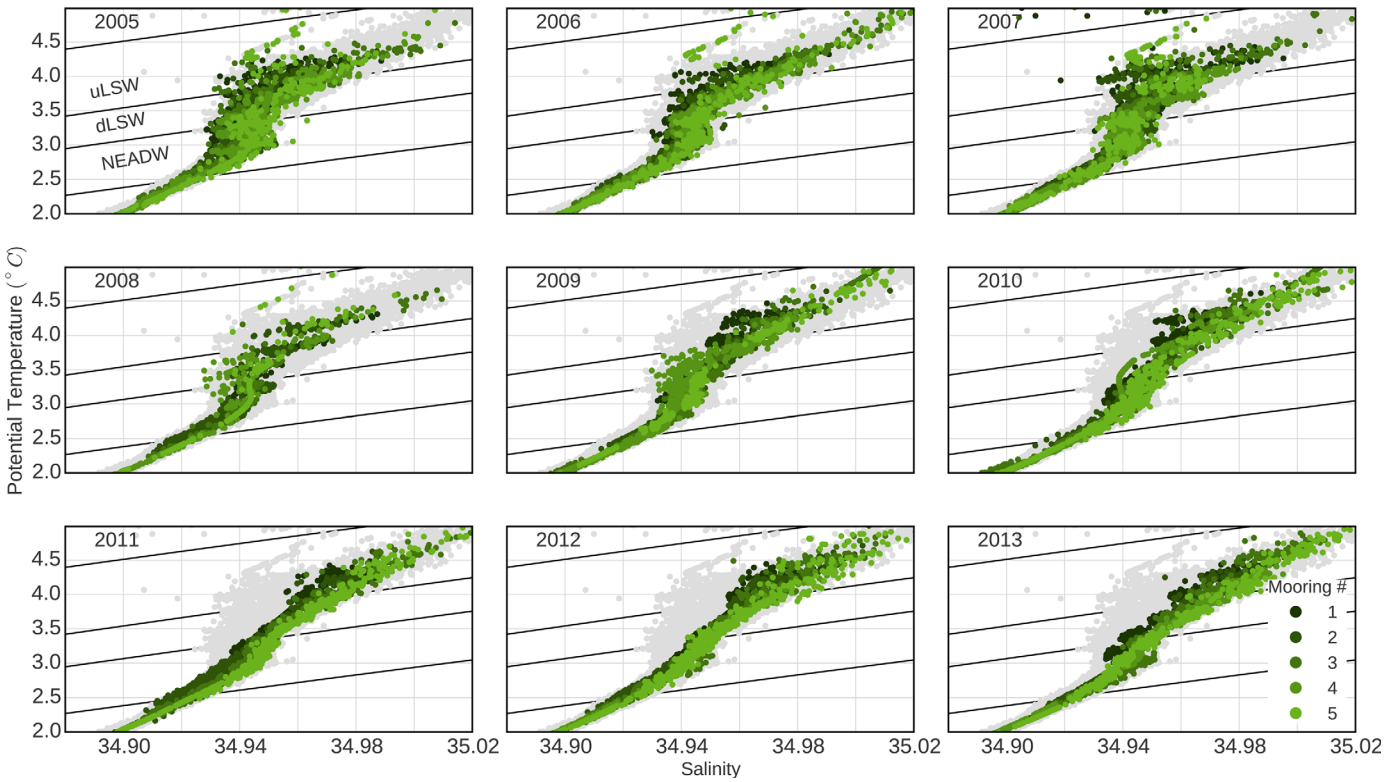

Figure 4. Evolution of θ-S properties at Line W moored array from 2005 to 2013. Gray background points are all profiles measured with 5 day resolution at Line W moorings w1–w5, and overlain green points are profiles measured in the year labeled in the top left of the plot. Moorings are differentiated by shades of green as described in the legend. There is a progression from a broad set of profiles spanning the measured θ-S space in 2005 to a focused concentration on the warm-salty edge of the measured θ-S space in 2013. There are fewer data in 2008 because of measurement gaps. Black lines are representative neutral density boundaries for 39°N and 1000 db.

discussed in more detail in section 6, the shift from a large range of properties to a narrow range (instead of a monotonic shift in properties from cold-fresh to warm-salty) is because there is a distribution of transit times from the Labrador Sea as well as stirring with the interior. Stirring with interior waters, which are generally warmer and saltier than the DWBC, also accounts for the fact that the properties at Line W are warmer and saltier and occupy a smaller range in θ-S space than the Labrador Sea θ-S properties do.

4. Correlation of Hydrographic Anomalies in Neutral Density Bins

Although a water mass property shift is observed at the Line W moorings that is consistent with changes in the Labrador Sea, the moored observations did not start early enough to record the first arrival of waters formed during the extreme deep convection event of the early 1990s. In order to quantify the correlation between the Labrador Sea and Line W data sets, we turn to the shipboard measurements, since there are at least yearly shipboard observations available from 1994 to 1997 as well as during the moored array period (2001–2014).

To gauge the correlation of the two data sets, we first switch to neutral density coordinates [*Jackett and McDougall*, 1997] so that the vertical coordinate for the Labrador Sea and Line W data are consistent and to remove the effects of heaving isopycnals. We calculate salinity and planetary potential vorticity (PPV) within 0.01 kg m^{-3} neutral density bins and then subtract the record mean of the time series within each bin. PPV is defined as f/h, where f is the Coriolis parameter at the data site and h is the vertical thickness of each neutral density bin. The data shown in Figure 5 and used in the subsequent analysis have been linearly interpolated in time. We do not show potential temperature because it mirrors salinity changes within neutral density bins.

To quantify the correlation between the anomaly time series shown in Figure 5, we computed the lagged correlation between the data sets within each 0.01 kg m^{-3} neutral density bin. The Labrador Sea and Line

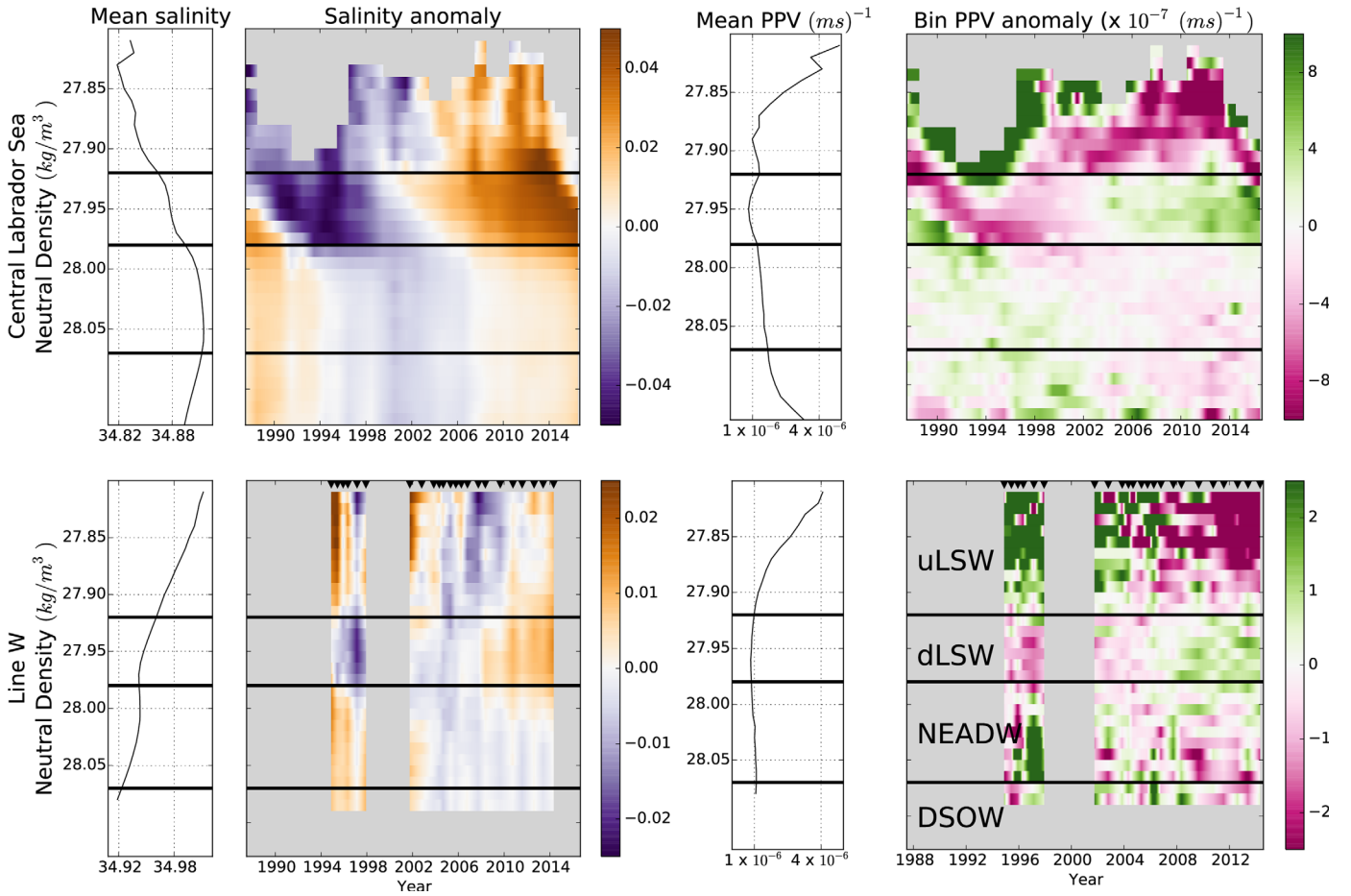

Figure 5. Water mass property anomaly time series and mean profiles (top row) in the central Labrador Sea and (bottom row) at Line W in neutral density space. Left plots show salinity anomalies within 0.01 kg m^{-3} neutral density bins and the corresponding mean profile on the left; the right plots show the same for PPV in neutral density space. Horizontal black lines are neutral density boundaries between water mass ranges, as labeled in the Line W PPV anomaly plot (bottom right). Black triangles at the top of Line W anomaly plots indicate when measurements were made. The colorbar ranges are larger for anomalies in the Labrador Sea than those at Line W.

W salinity and temperature anomalies are better correlated in the dLSW and NEADW density ranges than in uLSW density range (Figure 6a). PPV anomalies are better correlated in the dLSW density range than in the NEADW density range. This is likely because NEADW loses its PPV signature through entrainment in the subpolar gyre. None of these correlations are statistically significant since the anomaly time series are short compared to the event time scale and consequently have few degrees of freedom.

The lag which maximizes the correlation between potential temperature and salinity anomalies has a distinct structure in neutral density space (Figure 6b), with smaller lags in the dLSW density range than in the underlying NEADW range. This is consistent with *Yashayaev and Clarke* [2008], who found longer transit times for NEADW than LSW. This structure in neutral density space is visible in the Line W anomaly patterns in Figure 5; salinity and PPV anomalies vary similarly within the dLSW density range, but are distinct from anomalies in the uLSW and NEADW density ranges.

The final element of our lagged correlation analysis is the ratio of the magnitudes of lagged anomaly time series (Figure 6c). The standard deviations of the potential temperature, salinity, and PPV time series in the dLSW density range at Line W are about 0.2–0.3 times their original size in the Labrador Sea. This dilution of the original signal is to be expected, due to recirculation as well as stirring with other water masses on the way from the Labrador Sea to Line W. Because the extreme convection in the Labrador Sea from 1987 to 1994 was a unique input of a thick (low PPV), cold, and fresh layer into these intermediate densities, and because the travel times we find are consistent with other studies, as we will discuss further in section 7, this signal likely emanates from the Labrador Sea.

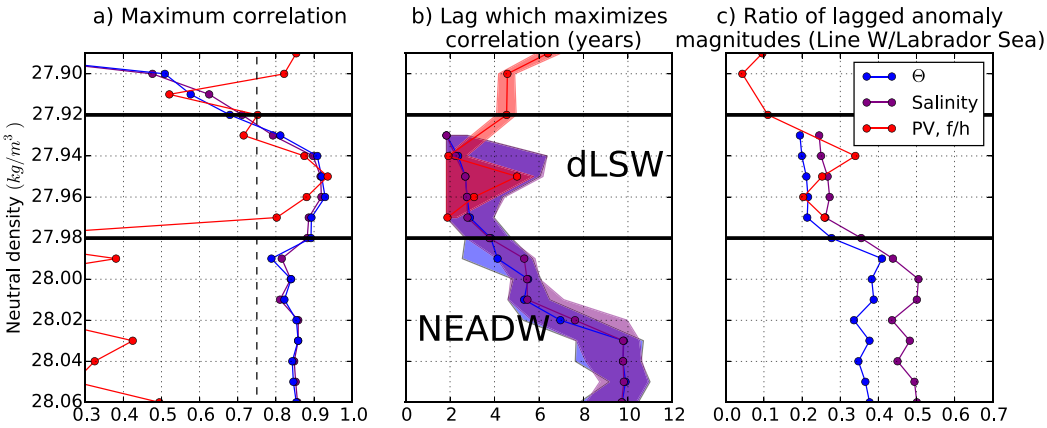

Figure 6. Results from lagged correlation analysis between Labrador Sea and Line W PPV, potential temperature, and salinity anomalies within neutral density bins (shown in Figure 5). The legend in Figure 6c applies to all plots. The horizontal black lines are neutral density boundaries between water mass density ranges, as labeled in Figure 6b. (a) Maximum correlation between Labrador Sea and Line W anomaly time series within the neutral density bins. The vertical dashed line indicates 0.75 and only bins with correlations higher than 0.75 are shown in the next panels. (b) The lag which yields the maximum correlation shown in Figure 6a. The envelope around the correlation-maximizing lag shows the range of lags which give more than 0.95 times this maximum correlation for each property. (c) Ratio of the standard deviations of the Labrador Sea and Line W lagged anomaly time series.

The variability in the uLSW and NEADW density ranges observed at Line W cannot be as directly linked with changes in the Labrador Sea. In the 2000s, less-extreme convection events are visible in the uLSW density range in the Labrador Sea (Figure 5). In the year 2000, convection reached 27.92 kg m^{-3}, or 1000 m, where a fresh and low PPV anomaly is apparent. These conditions continued for two more years, with convection reaching slightly deeper each year, forming $LSW_{2000–2003}$ [*Yashayaev*, 2007; *Yashayaev and Loder*, 2017]. The next deep-reaching convection event in 2008 [*Vage et al*., 2009; *Yashayaev and Loder*, 2009] is also perceptible, though its signature is very weak compared to the intense convection of the early 1990s. There is a general decline in PPV in the uLSW density range both in the Labrador Sea and at Line W throughout the 2000s (Figure 5), though it is not clear whether these changes are connected. There is potentially an indication of the arrival of $LSW_{2000–2003}$ as a low salinity, low PV signal in the late 2000s at Line W, but this is shrouded by other variability in the uLSW density range. The water mass property anomalies in the NEADW density range in the Labrador Sea are much smaller than those in the dLSW range, so are more easily obscured by stirring with the interior.

5. Deep Labrador Sea Water Properties Along the DWBC

To assess the along-path evolution of dLSW properties in the DWBC, we average within the dLSW layer, compare absolute quantities and include more measurement locations (Figures 1 and 7). The additional measurement locations that we analyze include a time series at the exit of the Labrador Sea at 53°N, where yearly shipboard hydrographic measurements have complemented a moored array across the DWBC since 1996 [*Dengler et al*., 2006; *Fischer et al*., 2010, 2015]. Our focus is on the shipboard data because they include salinity measurements. We include all profiles west of 48°W, which maximizes the consistency between sections and captures the DWBC. The second data set that we analyze in the subpolar gyre is further downstream at the Flemish Cap, at 47°N. We define the DWBC at the Flemish Cap as lying west of 43°W, which includes the DWBC on the continental slope as defined in *Mertens et al*. [2014] We also analyze three hydrographic sections off the Tail of the Grand Banks, in each case considering data out to the 3500 m isobath. Finally, in addition to the BATS data set 75 km southeast of Bermuda, introduced in section 3, we analyze the Hydrostation S data set, which is 25 km southeast of Bermuda [*Phillips and Joyce*, 2007].

The largest signal in the Labrador Sea is associated with the intense deep convection from 1987 to 1994 (Figures 5 and 7a). As the conditions for intense deep convection persisted, fresh surface properties were mixed down to greater densities, until about 1994, when the freshest dLSW properties were recorded (Figure 7a). Negative PPV anomalies can also be seen at ever denser densities throughout the early 1990s

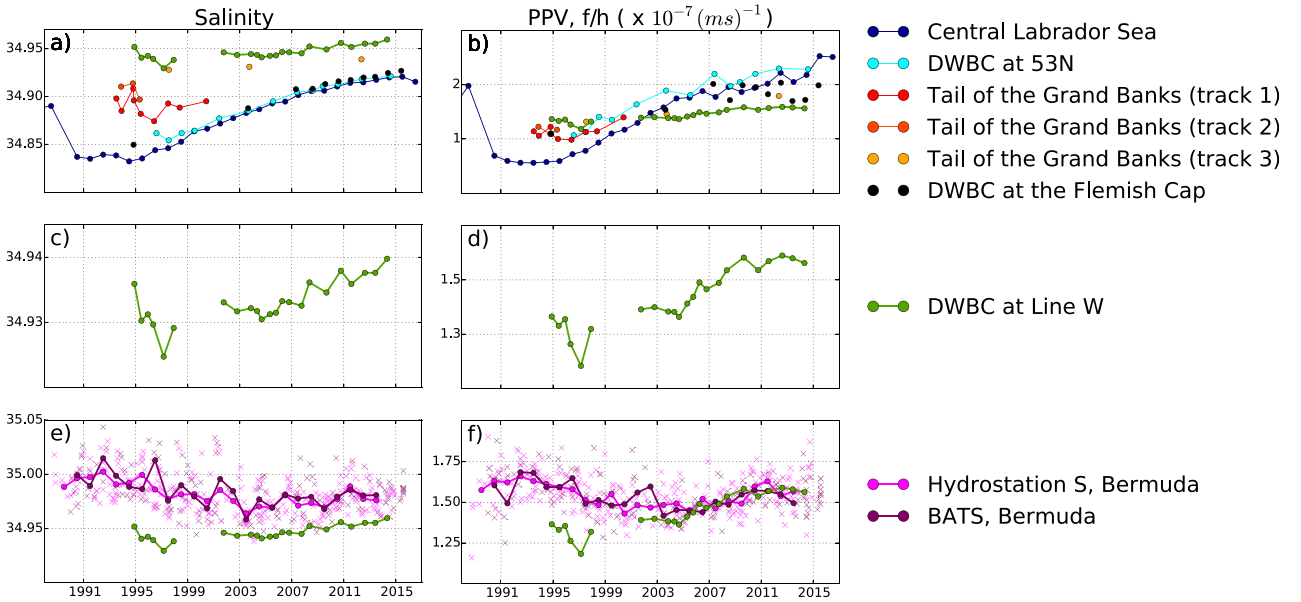

Figure 7. (left) Mean dLSW salinity and (right) PPV along the path of the DWBC. Rows correspond to different data locations: (a, b) subpolar gyre, (c, d) Line W, (e, f) Hydrostation S and BATS. Data sets are differentiated in the legends. Line W data are shown in each plot for comparison. The property time series in the subpolar gyre and Line W have similar shapes with a ≈5 year lag, reflecting the propagation of the fresh, low PPV anomaly associated with the early 1990s intense deep convection in the Labrador Sea.

(Figure 5). The PPV of the full dLSW density range reached a minimum in 1994 (Figure 7b), corresponding to layer thicknesses of over 2000 m. Subsequently, dLSW became saltier and PPV increased through the 2000s.

Downstream at Line W, there is a minimum in mean PPV and salinity in the dLSW density range, as in the Labrador Sea (Figure 5). In the late 1990s, a striking fresh anomaly was observed at Line W in the dLSW density range (Figures 5 and 7). Then, as in the Labrador Sea, the dLSW at Line W became saltier and PPV increased throughout the 2000s. These trends were recorded by the Line W moored array from 2004 to 2014 (w3 from 2001) with statistical significance (Figure 8). Salinity changes were consistent with an increase of 0.012 ± 0.004/decade, and a trend in potential temperature of $+0.014 \pm 0.004$°C/yr. There was also a statistically significant increase in dLSW PPV at Line W over this time period, which is equivalent to a decrease in dLSW layer thickness on the order of 10 ± 5 m/yr. Quoted uncertainties are 95% confidence intervals, as detailed in Appendix A. All trends and uncertainties are listed Table A1. Unlike in *Peña-Molino*

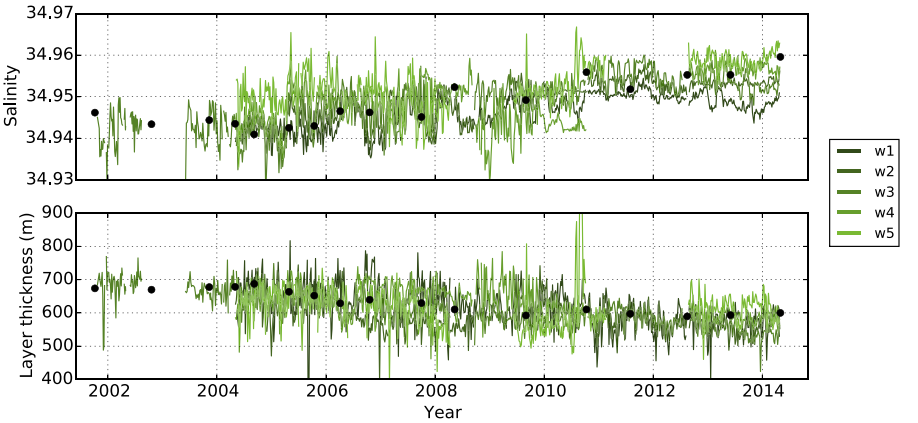

Figure 8. Mean dLSW salinity and layer thickness measured by Line W moorings, w1–w5 (locations in Figure 1). The legend shows which shade of green corresponds to which mooring measurement. The slope values and uncertainties of linear fits to these data are quoted in Table A1. Black dots are shipboard data for comparison. Shipboard salinity averages are weighted by layer thickness.

et al. [2010], warm core rings have not been removed from this record, and trends are significant despite their influence.

Increasing salinity and PPV after the deep convection period were observed throughout the subpolar gyre: at 53°N, the Flemish Cap and the Tail of the Grand Banks (Figure 7). Salinity and PPV increase along the path of the DWBC, as the uniquely fresh and low PPV waters formed by deep convection are stirred with waters of higher salinity and PPV. The largest changes in absolute salinity occur south of the Flemish Cap, indicating an increase of stirring with high-salinity waters. However, this along-path change is observed more consistently in dLSW salinity than PPV, because the absolute value of PPV is more sensitive to the details of its calculation. For example, the lateral PPV structure at each of the data sites is distinct, and we report the PPV of horizontally averaged properties at each location. In addition, most measurements in the subpolar gyre have a seasonal bias so that the true PPV minimum in winter was not necessarily measured.

The BATS and Hydrostation S dLSW salinity and PPV time series have high variability on monthly time scales. Nonetheless, there is some indication of a minimum in annual mean salinity and PPV at the end of 2003 (Figure 7e). This could be because of the slower and less consistent arrival of the cold-fresh, low PPV dLSW formed in the central Labrador Sea in the early 1990s, but we cannot show this conclusively here. The influence of LSW in shaping the water mass properties at Hydrostation S has been discussed by *Curry et al*. [1998], *Joyce et al*. [2000], and *Phillips and Joyce* [2007].

In summary, the intense convection of the early 1990s in the Labrador Sea formed a fresh and low PPV anomaly in the dLSW density range. This anomaly can be tracked throughout the subpolar gyre, and appears to arrive at Line W about 5 years later in 1997, albeit with decreased magnitude. While dLSW salinity is very consistent from the central Labrador Sea to the Flemish Cap, it is altered by the time it reaches the Tail of the Grand Banks and Line W, indicating that significant stirring occurs south of the Flemish Cap, as suggested by *Bower et al*. [2009].

6. Quantification of Water Mass Transit Time Distributions

6.1. Introduction to Model Framework

In order to assess whether the Labrador Sea and Line W water mass property time series are consistent with realistic advective and mixing time scales, we use the *Waugh and Hall* [2005] boundary current model framework. In the *Waugh and Hall* [2005] model, tracers with concentration χ are advected along a boundary current with a constant speed, u, and are mixed with a stagnant interior with time scale, t_{mix}. The simplified equations that describe their model are

$$\frac{\partial \chi_b}{\partial t} + u\frac{\partial \chi_b}{\partial x} + \frac{1}{t_{mix}}(\chi_b - \chi_i) = S_b, \tag{1}$$

$$\frac{\partial \chi_i}{\partial t} - \frac{\alpha}{t_{mix}}(\chi_b - \chi_i) = S_i, \tag{2}$$

where the subscript b denotes the property on the boundary and i in the interior; x is the along-boundary current coordinate; α is the ratio of the widths of the boundary and interior regions; S indicates a source term. Both χ_b and χ_i are functions of x and t.

A transit time distribution for a property propagating in the boundary can be associated with this model by solving equations (1) and (2) with a delta function boundary condition in the boundary current and no sources, i.e., $\chi_b(0,t)=\delta(t)$, $S_b=S_i=0$ [*Waugh and Hall*, 2005]. The ratio of the mixing time scale (t_{mix}) and the advective time scale ($t_{adv}=L/u$) shapes the transit time distribution; this ratio is the Peclet number, $Pe=t_{mix}/t_{adv}$. For $Pe \gg 1$, advection dominates over mixing and the transit time distribution approaches a delta function centered at t_{adv} as $Pe \to \infty$. For $Pe \ll 1$, mixing dominates and tends to broaden the transit time distribution, i.e., water parcels will take longer to travel down the DWBC as they are mixed with the interior.

In the next two subsections, we will gauge the consistency of the Labrador Sea and Line W water mass property time series with the *Waugh and Hall* [2005] model and calculate transit time distributions in two different ways: using an analytical solution for periodic tracer signals and a forward model approach. These

methods have complementary strengths and shortcomings and together show that the dLSW data are consistent with advective and mixing time scales which are on the same order.

6.2. Analytical Model

One way to assess whether the Labrador Sea and Line W time series are consistent with the model framework is to use the analytical solution that *Waugh and Hall* [2005] derive for a tracer with periodic boundary conditions. In order to apply this analytical solution, we assume that the entire time history of water mass potential temperature and salinity time series are periodic. As shown in Figure 9, the water mass potential temperature and salinity data are periodic to first order and there is evidence that they vary periodically on longer time scales [*Hurrell and Deser*, 2010].

To diagnose t_{mix} and t_{adv} and hence a transit time distribution between the Labrador Sea and Line W for dLSW, we fit sinusoids to the dLSW central Labrador Sea potential temperature and salinity time series from 1990 onward to capture the extreme deep convection event. We then fit sinusoids with the periods that we found from fitting the Labrador Sea data to the Line W dLSW potential temperature and salinity time series. From these fits, we have estimates of T_ω, the period of oscillation found from the Labrador Sea data fit, A_ω, the ratio of the amplitudes of the sinusoids fits to the Line W and Labrador Sea data, and t_ω, the phase shift between them. Because we are fitting a sinusoid with a set period to the data, the dLSW salinity minimum of the sinusoidal fit falls within the Line W data gap, unlike in section 4 in which we linearly interpolated over the data gap.

To find t_{mix}, we rearrange *Waugh and Hall*'s [2005] equations (10) and (11) to obtain the following quadratic equation:

$$t_{mix}^2 + \frac{t_\omega}{\ln(A_\omega)} t_{mix} + \frac{\alpha(\alpha+1)}{(2\pi/T_\omega)^2} = 0. \tag{3}$$

Because t_{mix} is the solution to a quadratic equation, there are either zero, one, or two possible values of t_{mix} for a given set of parameters. We use the solution for t_{mix} to derive a solution for t_{adv}:

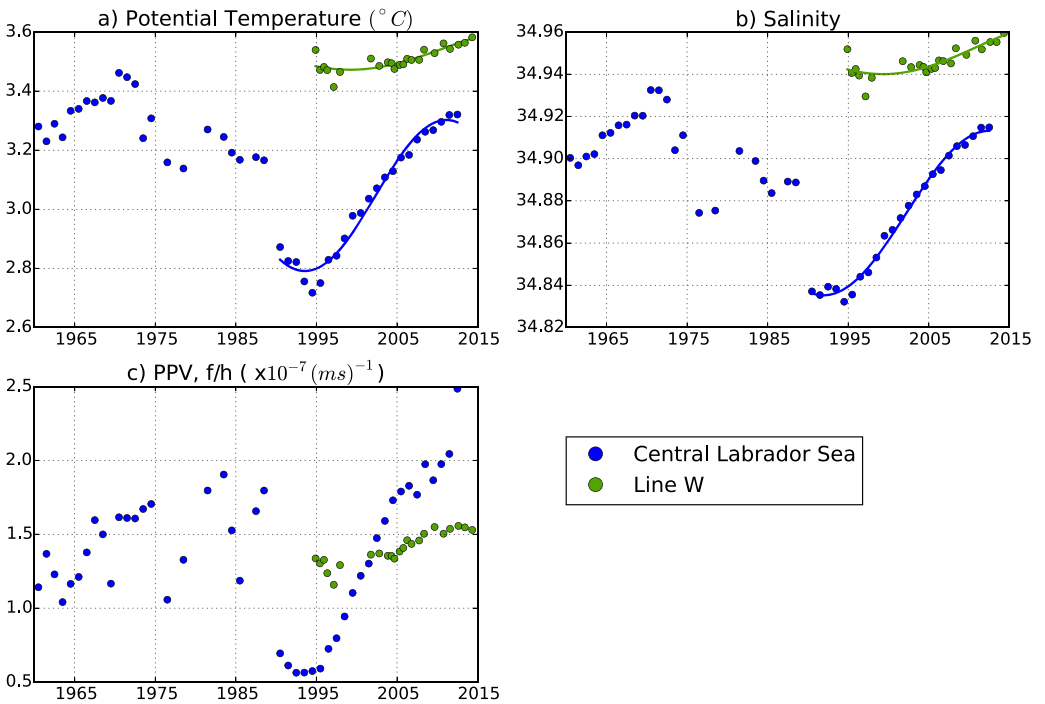

Figure 9. dLSW (a) potential temperature, (b) salinity, and (**c**) PPV in the Labrador Sea (blue) and at Line W (green). Lines indicate sinusoidal fits to central Labrador Sea and Line W dLSW potential temperature and salinity from 1990 onward used to find the analytical model solution. All data points are used to find the forward model fit.

Table 2. Parameters of Sinuisoidal Fits to Mean dLSW Properties and Resulting Solutions With $\alpha=0.1$[a]

	θ	S
Fit Parameters		
T_ω: period (years)	35	40
A_ω: relative amplitude	0.21	0.28
t_ω: phase shift (years)	5.8	7.3
Solutions		
t_{mix} (years)	1.4/2.3	0.9/4.8
t_{adv} (years)	2.4/3.8	1.7/6.3
u (cm/s)	5.5/3.5	8/2
$P=t_{mix}/t_{adv}$	0.58/0.62	0.53/0.76

[a]S refers to the dLSW salinity time series and θ to its potential temperature.

$$t_{adv}=t_\omega\frac{\alpha^2+r_\omega^2}{\alpha(\alpha+1)+r_\omega^2},\quad \text{where } r_\omega=2\pi t_{mix}/T_\omega. \tag{4}$$

Solving for t_{mix} and t_{adv} requires a choice of α, the ratio of the width of the boundary current to the interior. *Doney and Jenkins* [1994] found a range of α from 0.03 to 0.13 using a numerical model to match measured tritium and ^{3}He propagation in the North Atlantic. *Smith et al.* [2016] estimate $\alpha=0.1-0.4$ from CFC-11 decay scales at Line W. For consistency with *Waugh and Hall* [2005], we focus on $\alpha=0.1$ and discuss the α dependence of our results for context. An α of 0.1 implies an interior region that spans the western North Atlantic to the mid-Atlantic ridge for a 100 km wide DWBC.

The sinusoidal fits to the dLSW potential temperature and salinity data have periods, $T_\omega=35$ and 40 years, relative amplitudes, $A_\omega=0.21$ and 0.28, and phase shifts, $t_\omega=5.8$ and 7.3 years, respectively. We use equations (3) and (4) to solve for t_{mix} and t_{adv} for each set of parameters, as listed in Table 2, and focus here on the solutions which yield realistic DWBC velocities.

The differences between these fit parameters are likely due to nonlinearities in the equation of state for neutral density, as the water mass properties are averaged between neutral density contours. The relative contribution of salinity and temperature to neutral density changes both in time and space; salinity plays a larger role for colder water. The neutral density is more determined by salinity in the Labrador Sea than at Line W, especially during the period of extreme deep convection in early 1990s. Hence, though we follow dLSW from the Labrador Sea to Line W to first order, even the neutral density layer we follow is an imperfect neutral surface, probably because of the unique properties of this water mass.

The realistic set of solutions are $t_{adv}=3.8$ and 6.3 years and $t_{mix}=2.3$ and 4.8 years for dLSW potential temperature and salinity, respectively, which give Peclet numbers $Pe=0.62$ and 0.77. As the Peclet numbers are close to 1, these results imply that the roles of advection and mixing are of similar order, with a marginally greater role for mixing as $t_{mix}<t_{adv}$. The transit time distributions that correspond to these parameters have a dominant peak at t_{adv} and a long tail of transit times that extends well into 100 years (Figure 10). As discussed in *Waugh and Hall* [2005], the height of the dominant peak determines the degree of attenuation of the signal as it propagates and the tail can shift its phase further than the advective time scale.

Our solutions are dependent on the choice of α, the ratio between the boundary current and interior widths. For example, for a ratio half the size, $\alpha=0.05$, the set of realistic solutions are $t_{adv}=5.3$ and 6.9 years and $t_{mix}=3.4$ and 5.5 years for dLSW potential temperature and salinity, respectively, which have very

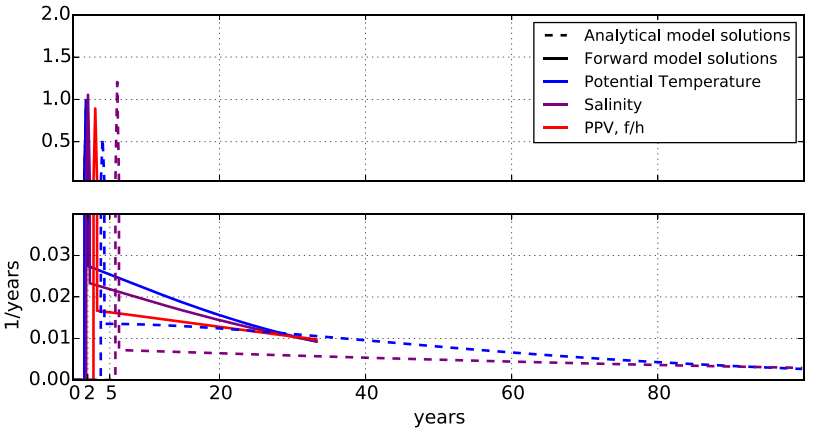

Figure 10. Range of potential transit time distributions solutions from the Labrador Sea to Line W for dLSW. Delta functions are normalized so that transit time distribution integrates to 1, as it is a probability density function. The bin size is 0.25 years, so that an advective peak with scale 1 implies a signal attenuation to 1/4 of its original size. The top and bottom plots have different *y* axis scales so that both the scale of the advective peak and tail are visible. Dashed lines correspond to analytical model solutions and solid lines to forward model solutions. Solutions for potential temperature, salinity, and PPV time series are shown in blue, purple, and red, respectively.

similar Peclet numbers to the α=0.1 solutions. However, for α=0.25, which was used in *Smith et al*. [2016], there are no solutions for our fit parameters.

The analytical solution to the *Waugh and Hall* [2005] framework requires the assumption of regular periodicity of water mass properties. To first order, we argue that the water mass data are periodic, and we are able to find consistent solutions for dLSW potential temperature and salinity evolution. The solutions indicate a first-order role for both advection and diffusion in the DWBC between the Labrador Sea and Line W with an advective time scale on the order of 5 years. In the next subsection, we describe an alternate approach to finding transit time distributions that does not require the assumption of regular periodicity.

6.3. Forward Model

An alternative approach to solving for t_{mix} and t_{adv} is to apply a forward model to the Labrador Sea data and assess how well it fits the Line W data. The advantage of this approach is that it does not require any assumptions about the character of the data time series or its history before measurements were made. However, because the Labrador Sea data set began 34 years before the Line W data set, this limits the length of the transit time distribution solution to 34 years (Figure 10).

To find a modeled downstream property time series, we apply

$$\chi_b(L,t)=\int_0^{T_{\max}} \chi_b(0,t-\xi)G(L,\xi)d\xi, \tag{5}$$

which is modified from *Waugh and Hall*'s [2005] equation (5) for a conserved tracer and a finite upstream time history. $\chi_b(0,t)$ is the upstream property time series in the central Labrador Sea, and $\chi_b(L,t)$ is the downstream property time series, meant to model the property time series at Line W. $G(L, t)$ is the Green's function for properties at Line W, or transit time distribution between the Labrador Sea and Line W, which is the function we are solving for. T_{max} is the time over which the Green's function can be integrated, so in this case, 34 years.

We apply equation (5) to the central Labrador Sea property time series with Green's functions solutions that correspond to a range of advective time scales and mixing time scales, t_{adv} and t_{mix}. The functional form of the Green's function solution to equations (1) and (2) can be found in *Waugh and Hall* [2005]. To assess how well the modeled downstream time series matches the Line W data, we calculate a cost function,

$$J=\sum(\chi_{LW}(t)'-\chi_b(L,t)')^2, \tag{6}$$

where $\chi_{LW}(t)'$ is the property anomaly time series observed at Line W and $\chi_b(L,t)'$ is the modeled anomaly time series. For both records, the anomaly time series is the difference between the time series and its own time mean. We consider anomalies because there is an offset between the mean Labrador Sea and Line W potential temperature and salinity which we do not model. This offset occurs because the interior is warmer and saltier than the boundary current. Because the values and distribution of interior properties are not well constrained, we focus on the evolution of the signal in the boundary current and how stirring affects the propagation of anomalies. This amounts to neglecting how the mean properties are affected in finding our solution. Possible additions to our implementation of the model to account for this offset are sources in the interior or an altered boundary condition for the interior at $x = 0$, but these would add both complexity and uncertainty to our interpretation.

The cost function is minimized for combinations of t_{adv} and t_{mix} that have Peclet numbers that are close to or less than one (Figure 11). This is true for each dLSW parameter anomaly time series: potential temperature, salinity and PPV. The advective and mixing time scales that minimize the cost function for dLSW temperature and salinity anomaly time series at Line W (with α=0.1 and 0.25 year resolution) are $t_{adv} = 2$ and 2.25 years and $t_{mix} = 1.5$ and 1.75 years, respectively, with Peclet numbers of $Pe = 0.75$ and 0.78. The Line W dLSW PPV cost function is minimized for $t_{adv} = 3$ years and $t_{mix} = 2$ years, or $Pe = 0.66$. These Peclet numbers agree well with those found using the analytic solution. As before, we find different travel times for salinity and temperature likely because temperature has a smaller effect on density in the colder Labrador Sea than at Line W. PPV signals propagate differently because PPV is a vertical derivative and is subject to erosion by vertical mixing as well as different boundary conditions than salinity and temperature. The disparity in travel time estimates amongst water properties may reflect how stirring with interior waters affects

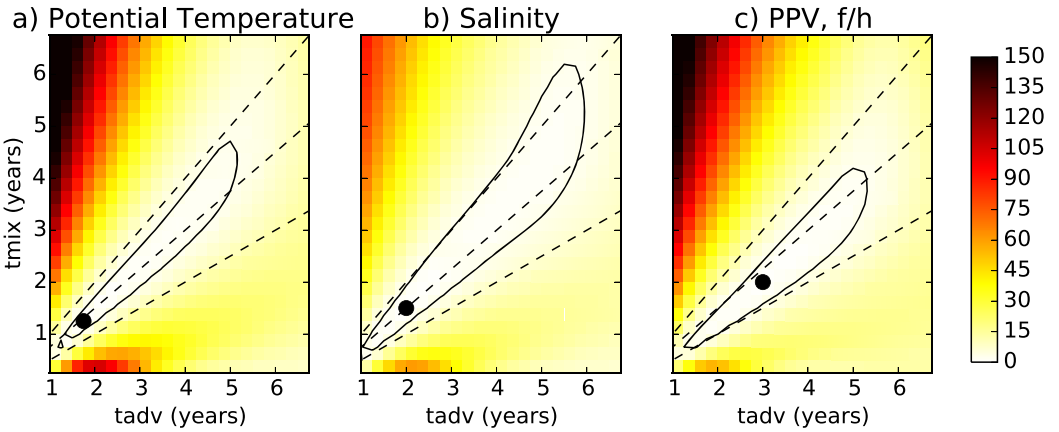

Figure 11. Cost functions for forward model fits to Line W dLSW (a) potential temperature, (b) salinity, and (c) PPV time series normalized by their minimum value, as a function of t_{adv} and t_{mix}. The black dot corresponds to the minimum cost function value for each property, and the black contour highlights range of solutions whose cost function are less than 3 times the minimum value found. The dashed lines are the $Pe = 1$, $Pe = 0.75$, and $Pe = 0.5$ lines for reference.

each property differently, changes in the source of waters arriving at Line W, or the wide range of potential travel times from the Labrador Sea to Line W.

Our results do not change significantly if a synthetic constant time history is added to extend the time over which the Green's function is integrated, or if single data points are removed from the Line W data set, i.e., no single data point is governing the fit. The result is most sensitive to removing the minimum dLSW potential temperature, salinity and PPV measurement in February 1997. Yet, even removing this point changes each of the time scales by less than 1 year, and all Peclet numbers are unchanged to within 0.1.

As was the case with the analytical model solutions, our results using the forward model approach are dependent on the choice of α, the ratio between the boundary current and interior widths. For a ratio half the size, α=0.05, the mean Peclet number for potential temperature, salinity and PPV solutions decreases to 0.68. For α=0.25, as used in *Smith et al.* [2016], $t_{adv} = 3$ years for the potential temperature and salinity data and 3.5 years for PPV and $t_{mix} = 2.5$ years for all variables, so that the mean Peclet number increases to 0.79. In other words, if the DWBC were broader with respect to the interior region (i.e., if α were greater) the best fit to the data would be given by a slower advection in the DWBC and less mixing. However, the size of α also affects the TTD, with larger α resulting in a greater proportion of transit times longer than the advective time scale.

The property anomaly time series modeled with the cost function minimizing parameters replicate the dLSW potential temperature, salinity and PPV minimum observed at Line W in the late 1990s as well the slopes before and after this extreme deep convection signal (Figure 12). However, because there is a data gap between 1999 and 2001, there is uncertainty as to the timing of the arrival of the deep convection

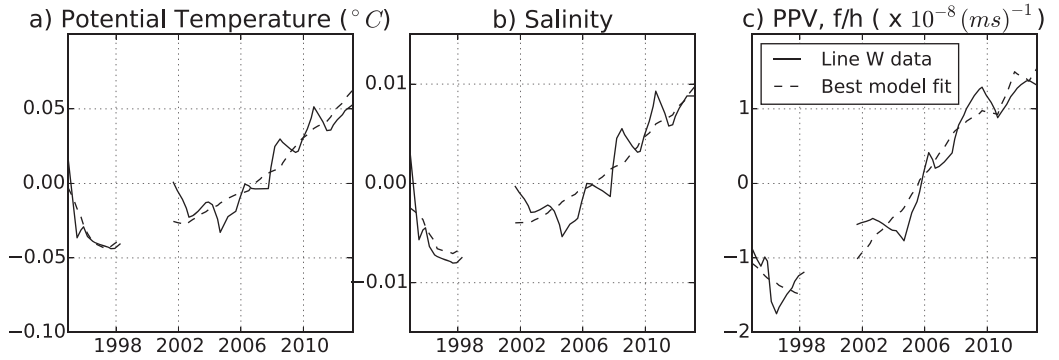

Figure 12. Best fits from the forward model to Line W dLSW (a) potential temperature, (b) salinity, and (c) PPV anomaly times series. Solid lines are linearly interpolated Line W dLSW property anomaly time series, and dashed lines are the property anomalies found by applying the best fit transit time distribution to Labrador Sea property time series. The best fit parameters, which minimize the cost function, are shown as black dots in Figure 11 and reported in the main text.

event, and these estimates of the advective time scale are likely biased short. An advective time scale of 2 years corresponds to a speed of 7 cm s^{-1}, which is faster than one would expect for a mean boundary current speed given direct velocity measurements of the DWBC. Indeed, the Peclet number is better constrained than the values of t_{adv} and t_{mix} using this method (Figure 11); i.e., there is a range of combinations of t_{adv} and t_{mix} which minimize the cost function, and a combination with a longer t_{adv} is more realistic. We find that t_{adv} and t_{mix} are on the same order using the forward model approach confirming the similar order role for advection and mixing we found using the analytical solution method.

We can also use our solutions to make an estimate of the bulk diffusivity, κ, between the DWBC and the interior as it travels from the Labrador Sea to Line W,

$$\kappa = \frac{l \times D}{t_{mix}}, \tag{7}$$

where l is the width of the DWBC and D is the distance between the Labrador Sea and Line W, as in *Doney and Jenkins* [1994]. For $l = 100$ km, $D = 4500$ km and $t_{mix} = 2.5$ years, $\kappa = 5700\,m^2\,s^{-1}$, which is on the same order as the *Ledwell et al*. [1998] estimate of $\kappa = 1000\,m^2\,s^{-1}$ in the eastern North Atlantic pycnocline. We might expect a higher value, as found here, along the western boundary of the North Atlantic, in the presence of strong eddy stirring. This bulk estimate is a parameterization of many processes, including recirculations, for example, and is specific to the estimation scale $O(100-1000\,km)$.

7. Conclusions

Observations of the DWBC at Line W reveal water mass changes that are consistent with changes in deep convection upstream in the Labrador Sea. We show trend reversals in potential temperature, salinity, and PPV at the Line W moored array that are consistent with the cessation of intense deep convection in the Labrador Sea and quantify the correlation between water mass property time series in neutral density space.

We draw on additional data sets to explore the evolution of water mass properties along the DWBC, using consistent neutral density water mass definitions throughout. We find that dLSW salinity is very similar from the Labrador Sea to the Flemish Cap, but is increased at the Tail of the Grand Banks, and increased further at Line W. The salinity minimum associated with the intense deep convection of the early 1990s can be tracked throughout these data sets, though the magnitude of variability in the record decreases as the signal propagates downstream. These findings are consistent with *Stramma et al*. [2004], who track water mass properties traveling through the northern subpolar gyre coherently, as well with *Bower et al*. [2009], who find high amounts of stirring between the boundary and the interior at the Tail of the Grand Banks.

Through a lagged correlation of dLSW potential temperature, salinity and PPV time series, we estimate a mean transit time between Line W and the Labrador Sea of 5 years, or a spreading rate of about 2.5 cm s^{-1} over a distance of 4500 km along the 3000 m isobath. There is significant uncertainty in this estimate because the shipboard measurements on which it is based are annual or semiannual. Because there is a 3 year data gap after the salinity minimum that we measure in 1997, this estimate may be fast; a fresher salinity minimum may have occurred during the 1999–2001 data gap.

Using the *Waugh and Hall* [2005] solution for the propagation of periodic signals in boundary currents, we estimated the transit time distribution of water parcels in the dLSW density range arriving at Line W from the Labrador Sea. Using an analytical solution for periodic tracers, we find a range of mixing time scales of $t_{mix} \approx 2.3-4.8$ years, and advective time scales of $t_{adv} \approx 3.8-6.3$ years. However, estimating the transit time distribution using this analytical solution requires the assumption of a periodic time history, and only sinusoidal fits to the Labrador Sea data from 1990 onward yielded physical results. Using a forward model applied to the Labrador Sea data yields $t_{mix} \approx 1.25-1.75$ years and $t_{adv} \approx 2-2.5$ years, which are likely underestimates due to the gap in the Line W data from 1999 to 2001. The dependence of the cost function on t_{adv} and t_{mix} (Figure 11) shows that this solution method constrains the Peclet number better than the absolute time scales; longer advective and mixing time scales are also good solutions. These two methods yield consistent solutions with Peclet numbers between 0.6 and 0.8 for dLSW water mass properties, implying that advection and diffusion play leading order roles in the propagation of water mass property signals in our dLSW density range. These solutions imply less mixing than *Waugh and Hall*'s [2005] $t_{mix} \approx 1$ year and hence a slower decay of water mass property signal amplitude in the DWBC.

Our transit time estimates are faster than *Peña-Molino et al*.'s [2010] estimate of 9 years for dLSW, which rested primarily on the timing of planetary potential vorticity minima and was limited by the starting time of Line W mooring w3 in 2001. Our estimate is consistent with other mean transit times along the boundary deduced from salinity anomalies on density surfaces; *Molinari et al*. [1998] and *Van Sebille et al*. [2011] both found a 10 year transit time for "classical" LSW from the Labrador Sea to the Abaco Line at 26.5°N, corresponding to a 2–2.5 cm s^{-1} spreading rate. However, *Molinari et al*. [1998] and *Van Sebille et al*. [2011] found ratios of water mass variability amplitude between the Abaco Line and the Labrador Sea of order 1 and 0.5, respectively. These amplitude ratios are larger than those we measure for dLSW salinity and temperature time series at Line W ($\approx 0.2-0.3$), which is upstream of Abaco. If the system can be modeled using an advective-diffusive model, it does not make sense that the signal would be larger at Abaco than at Line W.

Van Sebille et al. [2011] suggest that the preservation of the signal's amplitude may be explained by high mixing between the boundary and the interior, i.e., that the DWBC is in the fast mixing, fast advection limit described in *Waugh and Hall* [2005]. However, this would require mean DWBC advection speeds that are faster than any DWBC velocities that have been recorded, on the order of 50 cm s^{-1}. Further, it is unclear whether the *Waugh and Hall* [2005] model can be applied between the Labrador Sea and the Abaco line, because the DWBC has crossed underneath the Gulf Stream to get to Abaco. Some of the high salinity variance may be explainable through the influence of Mediterranean Overflow Water, and even Antarctic Intermediate Water (though it generally occupies lower densities). Strictly, our results cannot be compared directly because we have different water mass definitions, however there does appear to be an inconsistency here that is not resolved.

Comparisons with transit times deduced from other tracers can be misleading, as *Waugh and Hall* [2005] explain. In the intermediate mixing regime, which the DWBC is likely in, the spreading rate inferred from lagged correlations of tracer time series depends on the tracer initial conditions. Anthropogenic tracers (such as CFCs) which often have approximately exponential growth at the beginning of their time history, will be altered differently by a transit time distribution with a tail of long transit times than a tracer with a periodic time history, such as salinity in this case. For a tracer that has exponential growth, the tail of long transit times will act to flatten out the exponential curve that is measured downstream and cause an overestimate of transit times if it is not analyzed carefully. Conversely, for an oscillatory salinity time series upstream, this tail of long transit times will bring anomalies of both signs, preserving the shape of the signal though shifting its phase. The amplitude of the signal also decreases as it propagates downstream. Therefore, to measure transit times from salinity, a signal with a large amplitude is required upstream, such as the intense deep convection in the early 1990s. The advantage to diagnosing transit times from salinity is that measurements are more readily available and the effective propagation speeds are faster. The advantage to tracers with exponential time histories is that their high-latitude source is more certain, as they have very low concentrations in the interior subtropical gyre. A full picture can be put together by considering results from both types of tracers.

Smethie [1993] used CFC measurements to predict an along-boundary spreading rate of 0.8 cm s^{-1} for the LSW CFC maximum from the Labrador Sea to Line W and in a later study, $1-2$ cm s^{-1} for all DWBC water masses [*Smethie et al*., 2000]. *Doney and Jenkins* [1994] estimated a DWBC Tritium and Helium spreading rate $0.75-1.5$ cm s^{-1} from the Labrador Sea to the subtropical North Atlantic. These values are slower than our estimate likely because of stirring with water that has lower tracer concentration and because of recirculation, as these studies recognize. As explained above, because these tracers have approximately exponential time histories at the source, spreading rate estimates are likely to be biased slow.

Recently, *Rhein et al*. [2015] compiled 25 years of CFC data to make maps of age and fraction of young deep water. Their results imply a CFC transit time of 11 years for LSW to Line W along the boundary, which is, again, longer than our estimate. This is likely because their assumed transit time distribution does not have a tail of long transit times as we infer here. As they integrate many data sets, they are able to show that the spreading rate of LSW is not uniform throughout its path from the Labrador Sea to Line W. In fact, they show that spreading is slowest through the "transition zone" near the Flemish Cap, which is also indicated by our analysis of water mass properties along the path of the DWBC.

Smith et al. [2016] use the *Waugh and Hall* [2005] model to estimate t_{adv} and t_{mix} for DSOW from the Labrador Sea to Line W using CFC and Iodine measurements. Their results, $t_{adv} \approx 5-6$ years and $t_{mix} \approx 2-4$ years are not directly comparable with ours, $t_{adv} \approx 4-6$ years, $t_{mix} \approx 2-5$ years, as our estimate is for dLSW and

theirs is for DSOW. Nevertheless, our respective time scale estimates are similar, indicating that there may not be much variation with depth in along-boundary water mass spreading rates of North Atlantic DWBC waters.

Transit time distributions for LSW have been calculated using particle trajectories from several model products. Unlike the transit time distributions, we infer, their transit time distributions are generally broad without an early advective peak. *Lozier et al*. [2013] estimate a transit time distribution for LSW from the Labrador Sea to 25°N in the FLAME model with a broad peak centered around 25 years, which is a slower spreading rate than inferred in this work. *Zou and Lozier* [2016] use the same model to examine the export of floats from deep convection areas in the central Labrador Sea. They find that the mean age of floats that reach the subtropical boundary (close to Line W) is 22 ± 10 years, which is also much longer than the transit times we estimate. *Jackson et al*. [2016] estimate transit time distributions of LSW from the Labrador Sea to 26.5°N in the GloSea5 reanalysis product and find a peak at 7 years, which is closer to the time scales found in this work.

It is inherently challenging to compare our results with those from Lagrangian model studies because of the differences in approach. While Lagrangian model studies tend to focus on the spreading of particles from one point upstream, and will expose any deviations from a straightforward path along the boundary, our focus on measurements along the boundary will highlight any connectivity that is present. Further, water mass properties represent an integrated result. Individual particles that encounter stirring along the boundary will likely be drawn off the boundary, but the water mass as a whole may persist with modified properties. The only stirring that is present in our estimate has occurred to water parcels that have remained in or re-entered the boundary current.

We present evidence for an advective pathway for dLSW along the DWBC from the central Labrador Sea to the subtropical gyre boundary at Line W with a mean transit time of 5 years. As discussed, this is notably shorter than most modeled transit times. Since 2012, deep convection has been reaching ever greater depths in the central Labrador Sea, with 2000 m mixed layers recorded in 2016 [*Yashayaev and Loder*, 2017]. This offers a rare opportunity in oceanography to conduct a real-world experiment by awaiting the arrival of this new water mass ($LSW_{2012–2016}$) at Line W and obtaining an independent measure of this transit time, potentially clarifying model and observation disagreements about LSW spreading.

Appendix A: Mooring Data Trend Uncertainty Calculation

To find 95% confidence intervals for the trends in the Line W mooring data, we estimate the decorrelation time scales of the dLSW salinity, potential temperature and PPV time series measured by each mooring. The decorrelation time scale reported in Table A1 is twice the integral of the autocorrelation function to its first zero crossing. This method results in a conservative estimate of the confidence intervals for finite time series [*Firing*, 1989]. The effective degrees of freedom for a given time series is given by the ratio of the full length of the time series and the decorrelation time scale.

Table A1. Decorrelation Time Scales, Equivalent Degrees of Freedom, Trends, and 95% Confidence Intervals in dLSW Water Mass Properties Measured by Line W Moorings From April 2004 to May 2014 (November 2001 to May 2014 for w3)

	w1	w2	w3	w4	w5
Salinity					
Decorrelation time scale (days)	79	87	80	236	91
Equivalent degrees of freedom	46	42	60	15	40
Trend (/decade)	0.012	0.016	0.014	0.012	0.012
Confidence interval (/decade)	±0.002	±0.003	±0.003	±0.007	±0.004
Potential Temperature, θ					
Decorrelation time scale (days)	42	50	55	56	63
Equivalent degrees of freedom	86	72	83	66	57
Trend (°C/yr)	0.016	0.018	0.013	0.010	0.010
Confidence interval (°C/yr)	±0.003	±0.002	±0.004	±0.007	±0.008
Layer Thickness					
Decorrelation time scale (days)	17	185	102	49	
Equivalent degrees of freedom	208	20	45	74	
Trend (m/yr)	−12	−5	−7	−7	n/a
Confidence interval (m/yr)	±2	±5	±2	±4	n/a

The confidence intervals are given by

$$\pm(s_\epsilon t_{test})/[(N^*-1)^{1/2}s_x]$$

where $s_\epsilon =$ is the standard error of the y variable (i.e., salinity), s_x is the standard error of the x variable, N^* is the effective degrees of freedom and t_{test} is a constant specific to the t-distribution which depends on the effective degrees of freedom.

Acknowledgments
The Line W observations presented here are the product of many years of hard work by a large group of scientists and technical staff on land and at sea, and we wish to acknowledge their contribution. Since 2004, the Line W project has been funded by NSF grants OCE-0726720, 1332667, and 1332834. All Line W data are available through OceanSites as well as at the Line W website, http://www.whoi.edu/science/PO/linew/. We gratefully acknowledge the Atlantic Zone Off-shelf Monitoring Program (AZOMP) run by the Bedford Institute of Oceanography (Fisheries and Oceans Canada), which has occupied the AR7W line annually since 1990. Please see *Yashayaev and Loder* [2016] for Labrador Sea data location details. We thank Martin Visbeck, Jürgen Fischer, Johannes Karstensen, and Patricia Handmann for providing the hydrographic data at 53°N and for hosting I.A.L.B. during a productive visit to Kiel. Monika Rhein, Dagmar Kieke, and Christian Mertens provided the Flemish Cap data, and we are grateful for their involvement. Tail of the Grand Banks data were extracted from the Clivar and Carbon Hydrographic database (cchdo.ucsd.edu). BATS and Hydrostation S data were downloaded from the Bermuda Institute of Ocean Sciences website (bats.bios.edu). Finally, we wish to thank Amy Bower, Michael Spall, Glenn Flierl, and Steven Jayne for interesting discussions and feedback on earlier versions of this work.

References

Andres, M., J. M. Toole, D. J. Torres, W. M. Smethie, T. M. Joyce, and R. G. Curry (2015), Stirring by deep cyclones and the evolution of Denmark strait overflow water observed at line W, *Deep Sea Res., Part I*, *109*, 10–26.

Bower, A. S., and H. D. Hunt (2000), Lagrangian observations of the Deep Western Boundary Current in the North Atlantic Ocean: Part I: Large-scale pathways and spreading rates, *J. Phys. Oceanogr.*, *30*, 764–783.

Bower, A. S., M. S. Lozier, S. F. Gary, and C. W. Böning (2009), Interior pathways of the North Atlantic meridional overturning circulation, *Nature*, *459*, 243–247.

Bower, A. S., S. Lozier, S. F. Gary, M. S. Lozier, and S. F. Gary (2011), Export of Labrador Sea Water from the subpolar North Atlantic: A Lagrangian perspective, *Deep Sea Res., Part II*, *58*, 1798–1818.

Bower, A. S., R. M. Hendry, D. E. Amrhein, and J. M. Lilly (2013), Direct observations of formation and propagation of subpolar eddies into the Subtropical North Atlantic, *Deep Sea Res., Part II*, *85*, 15–41.

Curry, R. G., M. S. McCartney, and T. M. Joyce (1998), Oceanic transport of subpolar climate signals to mid-depth subtropical waters, *Nature*, *391*, 575–577.

Dengler, M., F. A. Schott, C. Eden, P. Brandt, J. Fischer, and R. J. Zantopp (2004), Break-up of the Atlantic deep western boundary current into eddies at 8°S, *Nature*, *432*, 1018–1020.

Dengler, M., J. Fischer, F. A. Schott, and R. Zantopp (2006), Deep Labrador Current and its variability in 1996–2005, *Geophys. Res. Lett.*, *33*, L21S06, doi:10.1029/2006GL026702.

Dickson, B., I. Yashayaev, J. Meincke, B. Turrell, S. Dye, J. Holfort, R. R. Dickson, and J. Brown (2002), Rapid freshening of the deep North Atlantic Ocean over the past four decades, *Nature*, *99*, 832–837.

Doney, S. C., and W. J. Jenkins (1994), Ventilation of the deep western boundary current and abyssal western North Atlantic: Estimates from tritium and 3He distributions, *J. Phys. Oceanogr.*, *24*, 638–659.

Dong, S., M. O. Baringer, G. J. Goni, C. S. Meinen, and S. L. Garzoli (2014), Seasonal variations in the South Atlantic Meridional Overturning Circulation from observations and numerical models, *Geophys. Res. Lett.*, *41*, 4611–4618.

Firing, E. (1989), Mean zonal currents below 1500 m near the equator, 159°V, *J. Geophys. Res.*, *94*, 2023–2028.

Fischer, J., M. Visbeck, R. Zantopp, and N. Nunes (2010), Interannual to decadal variability of outflow from the Labrador Sea, *Geophys. Res. Lett.*, *37*, L24610, doi:10.1029/2010GL045321.

Fischer, J., et al. (2015), Intra-seasonal variability of the DWBC in the western subpolar North Atlantic, *Prog. Oceanogr.*, *132*, 233–249.

Gary, S. F., M. S. Lozier, W. B. Claus, and A. Biastoch (2011), Deciphering the pathways for the deep limb of the Meridional Overturning Circulation, *Deep Sea Res., Part II*, *58*, 1781–1797.

Gary, S. F., M. S. Lozier, A. Biastoch, and C. W. Böning (2012), Reconciling tracer and float observations of the export pathways of Labrador Sea Water, *Geophys. Res. Lett.*, *39*, L24606, doi:10.1029/2012GL053978.

Hansen, B., and S. Osterhus (2000), North Atlantic - Nordic Seas exchanges, *Prog. Oceanogr.*, *45*, 109–208.

Hummels, R., P. Brandt, M. Dengler, J. Fischer, M. Araujo, D. Veleda, and J. V. Durgadoo (2015), Interannual to decadal changes in the western boundary circulation in the Atlantic at 11°S, *Geophys. Res. Lett.*, *42*, 7615–7622, doi:10.1002/2015GL065254.

Hurrell, J. W. (1995), Decadal trends in the North Atlantic Oscillation: Regional temperatures and precipitation, *Science*, *269*, 676–679.

Hurrell, J. W., and C. Deser (2010), North Atlantic climate variability: The role of the North Atlantic Oscillation, *J. Mar. Syst.*, *79*, 231–244.

Jackett, D. R., and T. J. McDougall (1997), A neutral density variable for the world's oceans, *J. Phys. Oceanogr.*, *27*, 237–263.

Jackson, L. C., K. A. Peterson, C. D. Roberts, and R. A. Wood (2016), Recent slowing of Atlantic overturning circulation as a recovery from earlier strengthening, *Nat. Geosci.*, *9*, 518–522.

Joyce, T. M., C. Deser, and M. A. Spall (2000), The relation between decadal variability of subtropical mode water and the North Atlantic Oscillation, *J. Clim.*, *13*, 2550–2569.

Joyce, T. M., J. Dunworth-Baker, R. S. Pickart, D. Torres, and S. Waterman (2005), On the Deep Western Boundary Current south of Cape Cod, *Deep Sea Res., Part II*, *52*, 615–625.

Kanzow, T., U. Send, W. Zenk, A. D. Chave, and M. Rhein (2006), Monitoring the integrated deep meridional flow in the tropical North Atlantic: Long-term performance of a geostrophic array, *Deep Sea Res., Part I*, *53*, 528–546.

Kanzow, T., U. Send, and M. McCartney (2008), On the variability of the deep meridional transports in the tropical North Atlantic, *Deep Sea Res., Part I*, *55*, 1601–1623.

Kieke, D., M. Rhein, L. Stramma, W. M. Smethie, D. A. LeBel, and W. Zenk (2006), Changes in the CFC inventories and formation rates of Upper Labrador Sea Water, 1997–2001, *J. Phys. Oceanogr.*, *36*, 64–86.

Kieke, D., B. Klein, L. Stramma, M. Rhein, and K. Peter (2009), Variability and propagation of Labrador Sea Water in the southern subpolar North Atlantic, *Deep Sea Res., Part I*, *56*, 1656–1674.

Köhler, J., C. Mertens, M. Walter, U. Stöber, M. Rhein, and T. Kanzow (2014), Variability in the internal wave field induced by the Atlantic Deep Western Boundary Current at 16°N, *J. Phys. Oceanogr.*, *44*, 492–516.

Lazier, J., R. Hendry, A. Clarke, I. Yashayaev, and P. Rhines (2002), Convection and restratification in the Labrador Sea, 1990–2000, *Deep Sea Res., Part I*, *49*, 1819–1835.

Lazier, J. R. N. (2001), Deep convection, in *Ocean Circulation and Climate: Observing and Modelling the Global Ocean*, pp. 634–643, Academic Press, Cambridge, Mass.

LeBel, D. A., et al. (2008), The formation rate of North Atlantic Deep Water and Eighteen Degree Water calculated from CFC-11 inventories observed during WOCE, *Deep Sea Res., Part I*, *55*, 891–910.

Le Bras, I. A. (2017), Dynamics of North Atlantic Western Boundary Currents, PhD thesis, MIT-WHOI Joint Program in Phys. Oceanogr., Woods Hole, Mass.

Ledwell, J., A. Watson, and C. Law (1998), Mixing of a tracer in the pycnocline, *J. Geophys. Res.*, *103*, 21,499–21,529.

Lozier, M. S., S. F. Gary, and A. S. Bower (2013), Simulated pathways of the overflow waters in the North Atlantic: Subpolar to subtropical export, *Deep Sea Res., Part II*, *85*, 147–153.

Lynn, R. J., and J. L. Reid (1968), Characteristics and circulation of deep and abyssal waters, *Deep Sea Res. Oceanogr. Abstr.*, *15*, 577–598.

Marshall, J., H. Johnson, and J. Goodman (2001), A study of the interaction of the North Atlantic Oscillation with ocean circulation, *J. Clim.*, *14*, 1399–1421.

Meinen, C. S., W. E. Johns, S. L. Garzoli, E. van Sebille, D. Rayner, T. Kanzow, and M. O. Baringer (2013a), Variability of the Deep Western Boundary Current at 26.5°N during 2004–2009, *Deep Sea Res., Part II*, *85*, 154–168.

Meinen, C. S., S. Speich, R. C. Perez, S. Dong, A. R. Piola, S. L. Garzoli, M. O. Baringer, S. Gladyshev, and E. J. D. Campos (2013b), Temporal variability of the meridional overturning circulation at 34.5°S: Results from two pilot boundary arrays in the South Atlantic, *J. Geophys. Res. Oceans*, *118*, 6461–6478, doi:10.1002/2013JC009228.

Mertens, C., M. Rhein, M. Walter, C. W. Boning, E. Behrens, D. Kieke, R. Steinfeldt, and U. Stober (2014), Circulation and transports in the Newfoundland Basin, western subpolar North Atlantic, *J. Geophys. Res. Oceans*, *119*, 7772–7793, doi:10.1002/2014JC010019.

Molinari, R. L., R. A. Fine, W. D. Wilson, R. G. Curry, J. Abell, and M. S. McCartney (1998), The arrival of recently formed Labrador Sea water in the Deep Western Boundary Current at 26.5°N, *Geophys. Res. Lett.*, *25*, 2249–2252.

Peña-Molino, B., T. M. Joyce, and J. M. Toole (2010), Recent changes in the Labrador Sea Water within the Deep Western Boundary Current southeast of Cape Cod, *Deep Sea Res., Part I*, *58*, 1019–1030.

Peña-Molino, B., T. M. Joyce, and J. M. Toole (2012), Variability in the Deep Western Boundary Current: Local versus remote forcing, *J. Geophys. Res.*, *117*, C12022, doi:10.1029/2012JC008369.

Phillips, H. E., and T. M. Joyce (2007), Bermuda's tale of two time series: Hydrostation S and BATS, *J. Phys. Oceanogr.*, *37*, 554–571.

Pickart, R. S., N. G. Hogg, and W. M. Smethie (1989), Determining the strength of the Deep Western Boundary Current using the Chlorofluoromethane ratio, *J. Phys. Oceanogr.*, *19*, 940–951.

Pickart, R. S., D. R. Watts, S. Pickart, and D. R. Watts (1990), Deep Western Boundary Current variability at Cape Hatteras, *J. Mar. Res.*, *48*, 765–791.

Pickart, R. S., M. A. Spall, and J. R. N. Lazier (1997), Mid-depth ventilation in the western boundary current system of the sub-polar gyre, *Deep Sea Res., Part I*, *44*, 1025–1054.

Rhein, M. (2000), Drifters reveal deep circulation, *Nature*, *407*, 30–31.

Rhein, M., D. Kieke, and R. Steinfeldt (2007), Ventilation of the upper Labrador Sea Water, 2003–2005, *Geophys. Res. Lett.*, *34*, L06603, doi:10.1029/2006GL028540.

Rhein, M., D. Kieke, S. Hüttl-Kabus, A. Roessler, C. Mertens, R. Meissner, B. Klein, C. W. Böning, and I. Yashayaev (2011), Deep water formation, the subpolar gyre, and the meridional overturning circulation in the subpolar North Atlantic, *Deep Sea Res., Part II*, *58*, 1819–1832.

Rhein, M., D. Kieke, and R. Steinfeldt (2015), Advection of North Atlantic Deep Water from the Labrador Sea to the southern hemisphere, *J. Geophys. Res. Oceans*, *120*, 2471–2487, doi:10.1002/2014JC010605.

Schott, F. A., R. Zantopp, M. Dengler, J. Fischer, and M. Wibaux (2004), Circulation and deep-water export at the western exit of the subpolar North Atlantic, *J. Phys. Oceanogr.*, *34*, 817–843.

Schott, F. A., J. Fischer, M. Dengler, and R. Zantopp (2006), Variability of the Deep Western Boundary Current east of the Grand Banks, *Geophys. Res. Lett.*, *33*, L21S07, doi:10.1029/2006GL026563.

Silverthorne, K. E., and J. M. Toole (2009), Seasonal kinetic energy variability of near-inertial motions, *J. Phys. Oceanogr.*, *39*, 1035–1049.

Smethie, W. M. (1993), Tracing the thermohaline circulation in the western North Atlantic using chlorofluorocarbons, *Prog. Oceanogr.*, *31*, 51–99.

Smethie, W. M., R. A. Fine, A. Putzka, and E. Peter (2000), Tracing the flow of North Atlantic Deep Water using chlorofluorocarbons, *J. Geophys. Res.*, *105*, 14,297–14,323.

Smith, J. N., W. M. Smethie, I. Yashayaev, R. Curry, and K. Azetsu-Scott (2016), Time series measurements of transient tracers and tracer-derived transport in the Deep Western Boundary Current between the Labrador Sea and the subtropical Atlantic Ocean at Line W, *J. Geophys. Res. Oceans*, *121*, 8115–8138, doi:10.1002/2016JC011759.

Srokosz, M. A., and H. L. Bryden (2015), Observing the Atlantic Meridional Overturning Circulation yields a decade of inevitable surprises, *Science*, *348*, 1255575.

Stramma, L., D. Kieke, M. Rhein, F. Schott, I. Yashayaev, and K. P. Koltermann (2004), Deep water changes at the western boundary of the subpolar North Atlantic during 1996 to 2001, *Deep Sea Res., Part I*, *51*, 1033–1056.

Swallow, J., and L. Worthington (1961), An observation of a deep countercurrent in the Western North Atlantic, *Deep Sea Res.*, *8*, 1–19.

Swift, J. H. (1984), The circulation of the Denmark Strait and Iceland-Scotland overflow waters in the North Atlantic, *Deep Sea Res., Part A*, *31*, 1339–1355.

Talley, L. D., and M. S. McCartney (1982), Distribution and Circulation of Labrador Sea Water, *J. Phys. Oceanogr.*, *12*, 1189–1205.

Toole, J. M., R. G. Curry, T. M. Joyce, M. McCartney, and B. Peña-Molino (2011), Transport of the North Atlantic Deep Western Boundary Current about 39°N, 70°W: 2004–2008, *Deep Sea Res., Part II*, *58*, 1768–1780.

Vage, K., R. S. Pickart, V. Thierry, G. Reverdin, C. M. Lee, B. Petrie, T. A. Agnew, A. Wong, and M. H. Ribergaard (2009), Surprising return of deep convection to the subpolar North Atlantic Ocean in winter 2007–2008, *Nat. Geosci.*, *2*, 67–72.

Van Aken, H. M., and C. J. De Boer (1995), On the synoptic hydrography of intermediate and deep water masses in the Iceland Basin, *Deep Sea Res., Part I*, *42*, 165–189.

Van Sebille, E., M. O. Baringer, W. E. Johns, C. S. Meinen, L. M. Beal, M. F. De Jong, and H. M. Van Aken (2011), Propagation pathways of classical Labrador Sea water from its source region to 26°N, *J. Geophys. Res.*, *116*, C12027, doi:10.1029/2011JC007171.

Waugh, D. W., and T. M. Hall (2005), Propagation of tracer signals in boundary currents, *J. Phys. Oceanogr.*, *35*, 1538–1552.

Wüst, G. (1935), Schichtung und Zirkulation des Atlantischen Ozeans. Die Stratosphaere., *Wissenschaftliche Ergebnisse der Deutschen Atlantischen Expedition auf dem Forschungs- und Vermessungsschiff "Meteor" 1925 – 1927*, *6*.

Yashayaev, I. (2007), Hydrographic changes in the Labrador Sea, 1960–2005, *Prog. Oceanogr.*, *73*, 242–276.

Yashayaev, I., and A. Clarke (2008), Evolution of North Atlantic Water Masses inferred from Labrador Sea salinity series, *Oceanography*, *21*, 30–45.

Yashayaev, I., and J. W. Loder (2009), Enhanced production of Labrador Sea Water in 2008, *Geophys. Res. Lett.*, *36*, L01606, doi:10.1029/2008GL036162.

Yashayaev, I., and J. W. Loder (2016), Recurrent replenishment of Labrador Sea Water and associated decadal-scale variability, *J. Geophys. Res. Oceans*, *121*, 8095–8114, doi:10.1002/2016JC012046.

Yashayaev, I., and J. W. Loder (2017), Further intensification of deep convection in the Labrador Sea in 2016, *Geophys. Res. Lett.*, *44*, 1429–1438, doi:10.1002/2016GL071668.

Yashayaev, I., H. M. van Aken, N. P. Holliday, and M. Bersch (2007), Transformation of the Labrador Sea Water in the subpolar North Atlantic, *Geophys. Res. Lett.*, *34*, L22605, doi:10.1029/2007GL031812.

Zou, S., and M. S. Lozier (2016), Breaking the linkage between Labrador Sea Water production and its advective export to the subtropical gyre, *J. Phys. Oceanogr.*, *46*, 2169–2182.